Supporting Information

Campiglio et al. 10.1073/pnas.1715997115

SI Materials and Methods

Cloning Procedures. The cloning of $Ca_V1.2$, STAC3-GFP, STAC1-GFP, GFP-$Ca_V1.2$, and GFP-$Ca_V2.1$ was previously described (1, 2). Sequence integrity of the all newly generated constructs was confirmed by sequencing (MWG Biotech).

pc-$Ca_V1.2$-NT_A. The N terminus of the $Ca_V2.1\alpha_1$ (α_{1A}) subunit was inserted into the respective position of the N terminus of $Ca_V1.2$ by splicing by overhang extension (SOE)-PCR as follows. The regions containing the N terminus of $Ca_V2.1$ (nucleotides 1–294) and part of the first repeat of $Ca_V1.2$ (nucleotides 463–1,363) were isolated with overlapping primers from human pβA-$Ca_V2.1$–2HA (FJ040507) (3) and pc-$Ca_V1.2$, respectively. The two separate PCR products were fused in a SOE-PCR. Finally, the SOE-PCR fragment was HindIII and BamHI digested and subsequently ligated into the corresponding sites of pc-$Ca_V1.2$, yielding pc-$Ca_V1.2$-NT_A.

pc-$Ca_V1.2$-I-II_A. The I-II loop of $Ca_V2.1$ (α_{1A}) was inserted into the respective position of the I-II loop of $Ca_V1.2$ by SOE-PCR as follows. Two regions of $Ca_V1.2$, one containing part of repeat I (nucleotides 1,153–1,305) and one containing part of repeat II (nucleotides 1,663–2,140) were isolated from pc-$Ca_V1.2$, while the I-II loop of $Ca_V2.1$ (nucleotides 1,081–1,461) was isolated from pβA-$Ca_V2.1$–2HA with overlapping primers. The three separate PCR products were fused in a SOE-PCR. Finally, the SOE-PCR fragment was BamHI and EcoRI digested and subsequently ligated into the corresponding sites of pc-$Ca_V1.2$, yielding pc-$Ca_V1.2$-I-II_A.

pc-$Ca_V1.2$-II-III_M. The II-III loop of $Ca_V1.1$ from *Musca domestica* (4) was inserted into the respective position of the II-III loop of $Ca_V1.2$ by SOE-PCR as follows. Two regions of $Ca_V1.2$, one containing part of repeat II (nucleotides 2,123–2,349) and one containing part of repeat III (nucleotides 2,791–3,251), were isolated from pc-$Ca_V1.2$, while the II-III loop of the *Musca* channel (nucleotides 2,002–2,313) was isolated from GFP-α1SkLM (5) with overlapping primers. The three separate PCR products were fused in a SOE-PCR. Finally, the SOE-PCR fragment was EcoRI and PmlI digested and subsequently ligated into the corresponding sites of pc-$Ca_V1.2$, yielding pc-$Ca_V1.2$-II-III_M.

pc-$Ca_V1.2$-III-IV_A. The III-IV loop of $Ca_V2.1$ (α_{1A}) was inserted into the respective position of the III-IV loop of $Ca_V1.2$ by SOE-PCR as follows. Two regions of $Ca_V1.2$, one containing part of repeat III (nucleotides 3,404–3,591) and one containing part of repeat IV (nucleotides 3,751–4,728) were isolated from pc-$Ca_V1.2$, while the III-IV loop of $Ca_V2.1$ (nucleotides 4,536–4,701) was isolated from pβA-$Ca_V2.1$–2HA with overlapping primers. The three separate PCR products were fused in a SOE-PCR. Finally, the SOE-PCR fragment was ApaI and BstEII digested and subsequently ligated into the corresponding sites of pc-$Ca_V1.2$, yielding pc-$Ca_V1.2$-III-IV_A.

pc-$Ca_V1.2$-Δ1800. The PCT of $Ca_V1.2$ (nucleotides 4,501–5,400) was amplified from pc-$Ca_V1.2$ with the reverse primer introducing a stop codon followed by a XhoI site after amino acid A1800. The PCR product was then digested with BstEII and XhoI and inserted in the corresponding sites of pc-$Ca_V1.2$, yielding pc-$Ca_V1.2$-Δ1800.

pc-$Ca_V1.2$-PCT_A-Δ1800. The first 165 amino acids of the PCT of $Ca_V2.1$ (α_{1A}) were inserted into the corresponding position (amino acids 1,507–1,668) of the PCT of $Ca_V1.2$ by SOE-PCR as follows. Two regions of $Ca_V1.2$, one containing part of repeat IV (nucleotides 4,226–4,518) and one encoding amino acids 1,672–1,800 of the C terminus (nucleotides 5,005–5,400) were isolated from pc-$Ca_V1.2$-Δ1800, while the region encoding amino acids 1,825–1,989 of the PCT of $Ca_V2.1$ (nucleotides 5,473–5,967) was isolated from pc-$Ca_V2.1$–2HA with overlapping primers. The three separate PCR products were fused in a SOE-PCR. Finally, the SOE-PCR fragment was EcoRV and XhoI digested and subsequently ligated into the corresponding sites of pc-$Ca_V1.2$-Δ1800, yielding pc-$Ca_V1.2$-PCT_A-Δ1800.

Chimera A. The first 97 amino acids of the PCT of $Ca_V2.1$ (α_{1A}) were inserted into the corresponding position (amino acids 1,507–1,603) of the PCT of $Ca_V1.2$ by SOE-PCR as follows. One region containing the end of repeat IV (nucleotides 4,226–4,518) of $Ca_V1.2$ followed by region A of the C terminus of $Ca_V2.1$ (encoding amino acids 1,825–1,921) was isolated from pc-$Ca_V1.2$-PCT_A-Δ1800, while another region containing the remaining 197 amino acids of the PCT of $Ca_V1.2$ (nucleotides 4,810–5,400) was isolated from pc-$Ca_V1.2$-Δ1800 with overlapping primers. The two separate PCR products were fused in a SOE-PCR. Finally, the SOE-PCR fragment was EcoRV and XhoI digested and subsequently ligated into the corresponding sites of pc-$Ca_V1.2$-Δ1800, yielding pc-$Ca_V1.2$-PCT_A-CHIMERA A-Δ1800.

Chimera B. Forty amino acids of the PCT of $Ca_V2.1$ (α_{1A}) were inserted into the corresponding position (amino acids 1,604–1,640) of the PCT of $Ca_V1.2$ by SOE-PCR as follows. Two regions of $Ca_V1.2$, one containing the end of repeat IV and the beginning of the C terminus (nucleotides 4,226–4,920) of $Ca_V1.2$ and one containing the end of the PCT of $Ca_V1.2$ (nucleotides 4,930–5,400) were isolated from pc-$Ca_V1.2$-Δ1800, while another region encoding amino acids 1,922–1,961 of $Ca_V2.1$ was isolated from pc-$Ca_V1.2$-PCT_A-Δ1800 with overlapping primers. The three separate PCR products were fused in a SOE-PCR. Finally, the SOE-PCR fragment was EcoRV and XhoI digested and subsequently ligated into the corresponding sites of pc-$Ca_V1.2$-Δ1800, yielding pc-$Ca_V1.2$-PCT_A-CHIMERA B-Δ1800.

Chimera C. Twenty-eight amino acids of the PCT of $Ca_V2.1$ (α_{1A}) were inserted into the corresponding position (1,641–1,668) of the PCT of $Ca_V1.2$ by SOE-PCR as follows. One region containing the end of repeat IV and the beginning of the C terminus (nucleotides 4,226–4,920) of $Ca_V1.2$ was isolated from pc-$Ca_V1.2$-Δ1800, while another region containing amino acids 1,962–1,989 of $Ca_V2.1$ and the amino acids 1,672–1,800 of the C terminus of $Ca_V1.2$ was isolated from pc-$Ca_V1.2$-PCT_A-Δ1800 with overlapping primers. The two separate PCR products were fused in a SOE-PCR. Finally, the SOE-PCR fragment was EcoRV and XhoI digested and subsequently ligated into the corresponding sites of pc-$Ca_V1.2$-Δ1800, yielding pc-$Ca_V1.2$-PCT_A-CHIMERA C-Δ1800.

pc-$Ca_V1.2$-Δ1800-IQ Mutants. The single mutations of each of the 21 amino acids of the IQ domain of $Ca_V1.2$ to alanine were introduced by SOE-PCR as follows. Briefly, the PCT sequence of $Ca_V1.2$ was amplified by PCR with overlapping mutagenesis primers in separate PCR reactions using pc-$Ca_V1.2$-Δ1800 as a template. The two separate PCR products were then used as templates for a final PCR with flanking primers to connect the nucleotide sequences. This fragment was EcoRV and XhoI digested and cloned in the respective sites of pc-$Ca_V1.2$-Δ1800, yielding pc-$Ca_V1.2$-Δ1800-X16xxA.

GFP-$Ca_V1.2$-IQ_A. The region encoding $Ca_V1.2$ with the 28 amino acids from $Ca_V2.1$ was isolated from chimera C (which lacks the distal C terminus) with HindIII and AhdI and inserted in the corresponding sites of GFP-$Ca_V1.2$, yielding GFP-$Ca_V1.2$-IQ_A.

pc-STAC1, pc-STAC2, and pc-STAC3. The coding sequence of each STAC proteins was isolated from STACX-GFP with a reverse primer introducing a XhoI site. Each PCR products were then digested and inserted in the corresponding sites of the pc vector, yielding pc-STAC1, pc-STAC2, and pc-STAC3.

Dysgenic Myotubes Culture and Transfection. Myotubes of the homozygous dysgenic (*mdg*/*mdg*) cell line GLT were cultured as previously described (6). Cells grown on carbon and gelatin-coated coverslips were transiently transfected with the plasmids of interest 4 d after plating using FuGeneHD transfection reagent (Promega), according to the manufacturer's instructions.

Immunostaining and Image Processing. Paraformaldehyde-fixed cultures were immunolabeled as previously described (1) with rabbit polyclonal anti-GFP (1:10,000; Molecular Probes) and mouse monoclonal anti-β_1 (1:2,000, cl. N7/18, NeuroMab, University of California, Davis/National Institutes of Health NeuroMab Facility) and fluorescently labeled with secondary goat anti-rabbit Alexa-488 and goat anti-mouse Alexa-594 (1:4,000; Molecular Probes), respectively. Preparations were analyzed on an AxioImager microscope (Carl Zeiss) using 63× 1.4 NA objective. Fourteen-bit images were recorded with a cooled CCD camera (SPOT; Diagnostic Instruments) and Metaview image-processing software (Universal Imaging). Figures were arranged in Adobe Photoshop CS6 and, where necessary, linear adjustments were performed to correct black level and contrast. Semiquantative analysis of STAC3 coclustering was performed as previously described (1), by systematically screening for myotubes with more than four nuclei and clustered $Ca_V\beta_1$ in the red channel, which also expressed STAC3-GFP. According to the subcellular distribution of STAC3-GFP, each of these myotubes was classified as STAC3, coclustered or not. Results are expressed as mean ± SEM. All data were organized in MS Excel and analyzed using Student's *t* test or ANOVA with Tukey post hoc analysis in SPSS statistical software (SPSS).

Electrophysiology Recordings and Data Analysis. The tsA201 cells used already expressed human β_3 and $\alpha_2\delta$-1 subunits and were cultured as previously described (7). For electrophysiological recordings, tsA201 cells were transiently transfected with the GFP-tagged calcium channel in combination with a STAC isoform, if indicated, using FugeneHD (Promega), according to the manufacturer's instructions. The following day cells were replated on 35-mm culture dishes coated with poly-L-lysine. Cells were then kept at 30 °C and 5% CO_2 and used for electrophysiological recordings about 48–72 h after transfection. Dysgenic myotubes were transiently transfected with the GFP-tagged calcium channel using FugeneHD (Promega) and used for electrophysiological recordings 3–4 d after transfection.

Currents were recorded using the whole-cell patch clamp technique in voltage-clamp mode using an Axopatch 200B amplifier (Axon Instruments). Patch pipettes (borosilicate glass; Warner Instruments) had a resistance between 1.5 and 3 MΩ. For recordings of tsA201 cells, patch pipettes were filled with 144.5 mM Cs-Cl, 1 mM $MgCl_2$, 10 mM Hepes, 0.5 or 10 mM Cs-EGTA, and 4 mM Na_2-ATP (pH 7.4 with Cs-OH). For recordings of dysgenic myotubes: 145 mM Cs-aspartate, 2 mM $MgCl_2$, 10 mM Hepes, 0.1 mM Cs-EGTA, and 2 mM Mg-ATP (pH 7.4 with CsOH). For the recording of calcium currents from tsA201 cells, the cells were bathed in solution containing: 15 mM $CaCl_2$, 150 mM Choline chloride, 1 mM $MgCl_2$, and 10 mM Hepes (pH 7.4 with Cs-OH). Bath solution for barium currents recordings contained: 15 mM $BaCl_2$, 150 mM Choline chloride, 1 mM $MgCl_2$, and 10 mM Hepes (pH 7.4 with tetraethylammonium hydroxide). For the recording of the calcium currents form dysgenic myotubes, the myotubes were bathed in solution containing: 10 mM $CaCl_2$, 145 mM tetraethylammonium chloride, and 10 mM Hepes (pH 7.4 with tetraethylammonium hydroxide). Data acquisition and command potentials were controlled by Clampex software (v10.6; Axon Instruments); analysis was performed using Clampfit 10.5 (Axon Instruments) and Sigma-Plot 8.0 (SPSS Science) software. The current-voltage relationships were obtained by applying a 500-ms-long square pulse to various test potentials in 10-mV steps, starting from a holding potential of −80 mV. Because it was shown that the strength of inactivation correlates with the amplitude of the currents (8), only measurements in which the peak current was in the 200- to 3,000-pA range were analyzed (for Fig. S5, 900–3,000 pA). The resulting *I-V* curves were fitted according to $I = G_{max}\ (V - V_{rev})/(1 + \exp[-(V - V_{0.5})/k_a])$, where G_{max} is the maximum conductance of the slope conductance, V_{rev} is the extrapolated reversal potential of the calcium current, $V_{0.5}$ is the potential for half-maximal conductance, and k_a is the slope factor. The conductance was calculated using $G = (-I \times 1{,}000)/(V - V_{rev})$, and its voltage dependence was fitted according to a Boltzmann distribution: $G = G_{max}/(1 + \exp[-(V - V_{0.5})/k_a])$. Channel inactivation was measured by calculating the fractional inactivation (I_{res250}/I_{pk}) 250 ms from the peak of a 500-ms pulse from a holding potential of −80 mV to V_{max}, where V_{max} is the voltage leading to the peak current. Net CDI was determined by dividing the normalized calcium current by the average normalized barium current (9, 10). All quantitative data are expressed as mean ± SEM. Statistical significance was determined by unpaired *t* test or one-way ANOVA followed by Tukey post hoc analysis, as indicated using GraphPad Prism. Significance was set to $P < 0.05$.

1. Campiglio M, Flucher BE (2017) STAC3 stably interacts through its C1 domain with CaV1.1 in skeletal muscle triads. *Sci Rep* 7:41003.
2. Grabner M, Dirksen RT, Beam KG (1998) Tagging with green fluorescent protein reveals a distinct subcellular distribution of L-type and non-L-type Ca2+ channels expressed in dysgenic myotubes. *Proc Natl Acad Sci USA* 95:1903–1908.
3. Watschinger K, et al. (2008) Functional properties and modulation of extracellular epitope-tagged Ca(V)2.1 voltage-gated calcium channels. *Channels (Austin)* 2: 461–473.
4. Grabner M, et al. (1994) Insect calcium channels. Molecular cloning of an alpha 1-subunit from housefly (*Musca domestica*) muscle. *FEBS Lett* 339:189–194.
5. Wilkens CM, Kasielke N, Flucher BE, Beam KG, Grabner M (2001) Excitation-contraction coupling is unaffected by drastic alteration of the sequence surrounding residues L720-L764 of the alpha 1S II-III loop. *Proc Natl Acad Sci USA* 98: 5892–5897.
6. Powell JA, Petherbridge L, Flucher BE (1996) Formation of triads without the dihydropyridine receptor alpha subunits in cell lines from dysgenic skeletal muscle. *J Cell Biol* 134:375–387.
7. Ortner NJ, et al. (2017) Lower affinity of isradipine for L-type Ca2+ channels during substantia nigra dopamine neuron-like activity: Implications for neuroprotection in Parkinson's disease. *J Neurosci* 37:6761–6777.
8. Brunet S, Scheuer T, Catterall WA (2009) Cooperative regulation of Ca(v)1.2 channels by intracellular Mg(2+), the proximal C-terminal EF-hand, and the distal C-terminal domain. *J Gen Physiol* 134:81–94.
9. Barrett CF, Tsien RW (2008) The Timothy syndrome mutation differentially affects voltage- and calcium-dependent inactivation of CaV1.2 L-type calcium channels. *Proc Natl Acad Sci USA* 105:2157–2162.
10. Findeisen F, Minor DL, Jr (2009) Disruption of the IS6-AID linker affects voltage-gated calcium channel inactivation and facilitation. *J Gen Physiol* 133:327–343.

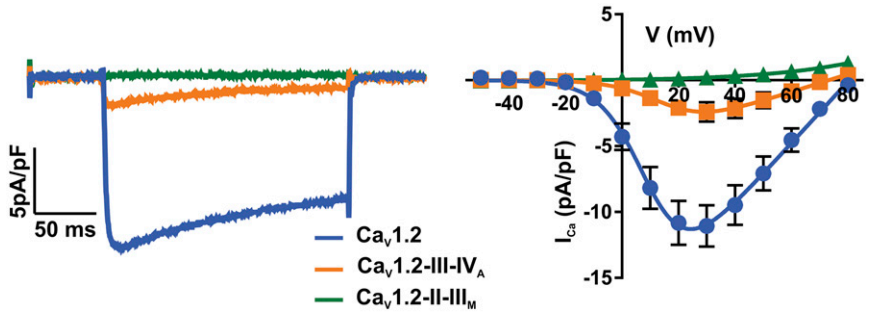

Fig. S1. The two chimeras showing no triad targeting in dysgenic myotubes display reduced current amplitude. Representative peak calcium currents (*Left*) and *I-V* relationships (*Right*) of Ca$_V$1.2-II-III$_M$ and Ca$_V$1.2-III-IV$_A$ compared with those of Ca$_V$1.2 (n = 5 for each construct).

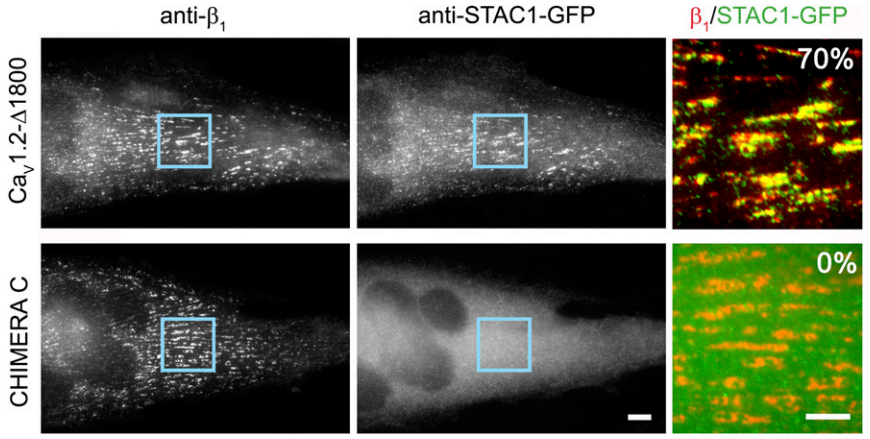

Fig. S2. STAC1 requires aa 1,641–1,668 to associate with Ca$_V$1.2 in the triads of dysgenic myotubes. Ca$_V$1.2-Δ1800 recruited STAC1-GFP to the channel complex by in 70% of the transfected myotubes, while chimera C, specifically lacking the IQ domain, failed to recruit STAC1 in all myotubes, indicating that the STAC interaction domain is conserved between STAC3 and STAC1 (n = 3, n = 90). Color overlay: 4× of blue rectangle. [Scale bars, 10 μm (*Left*) and 5 μm (*Right*).]

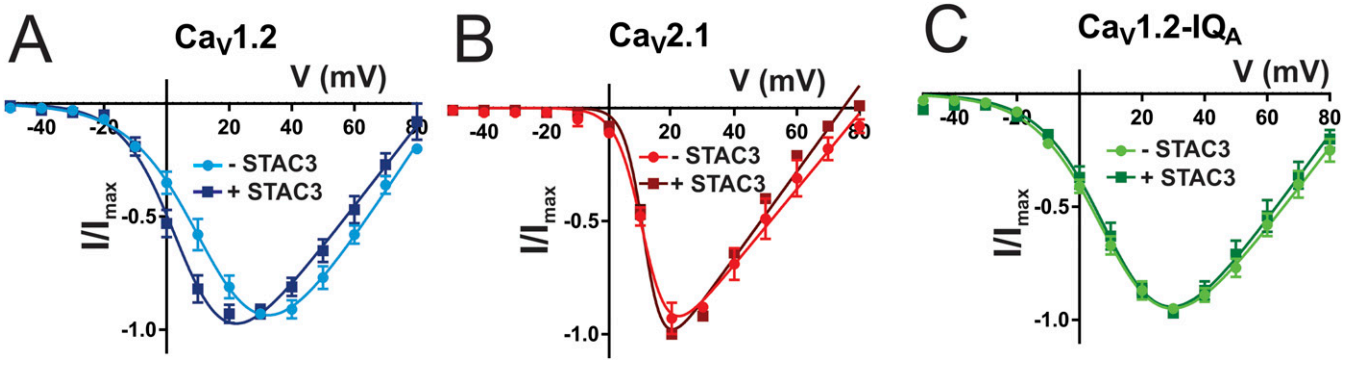

Fig. S3. Biophysical properties of Ca$_V$1.2, Ca$_V$2.1 and Ca$_V$1.2-IQ$_A$ with and without STAC3. Normalized current-voltage (IV) relationships of (*A*) Ca$_V$1.2 in the absence (light blue) or in the presence (dark blue) of STAC3, (*B*) Ca$_V$2.1 in the absence (red) or in the presence (dark red) of STAC3, (*C*) Ca$_V$1.2-IQ$_A$ in the absence (green) or in the presence (dark green) of STAC3. Unpaired t test shows no significant difference in the $V_{0.5}$ values. The fit parameters are reported in Table S3.

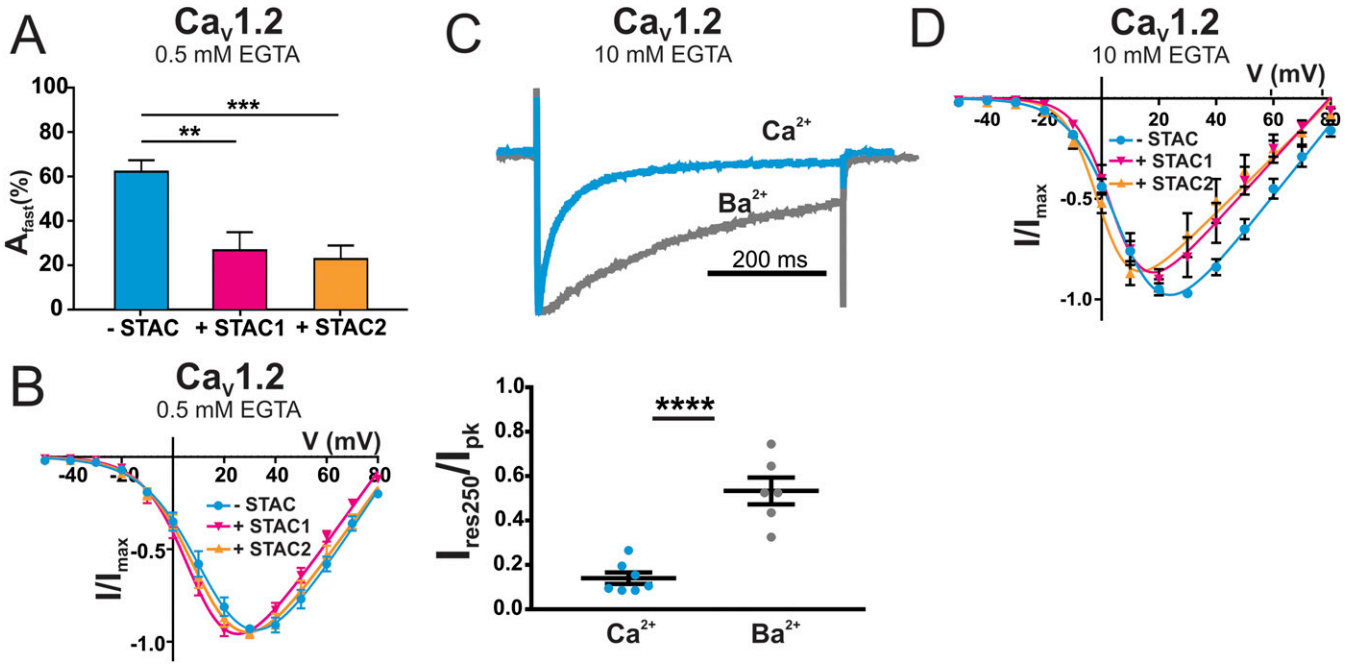

Fig. S4. Biophysical properties of $Ca_V1.2$ in the absence or presence of STAC1 and STAC2. (*A*) A_{fast}, the relative amplitude of the fast inactivation component for $Ca_V1.2$ calcium currents decreased significantly in the presence of STAC1 (magenta) and STAC2 (orange) compared with $Ca_V1.2$ calcium currents measured in the absence of a STAC protein (blue) ($[A_{fast}]_{-STAC} = 62.0 \pm 5.1\%$, $n = 11$, $[A_{fast}]_{+STAC1} = 26.5 \pm 8.2\%$, $n = 8$, $[A_{fast}]_{+STAC2} = 22.6 \pm 6.1\%$, $n = 9$). ANOVA $F_{(2, 24)} = 13.38$; $P = 0.0001$; *P* values in the figure are from Tukey post hoc analysis (**$P = 0.0017$, ***$P = 0.0003$). Normalized current-voltage (IV) relationships of $Ca_V1.2$ in the presence of STAC1 (magenta), STAC2 (orange), or in the absence of a STAC protein (light blue) in 0.5 mM EGTA (*B*) or 10 mM EGTA (*D*). The fit parameters are reported in Table S3. (*C*) Representative normalized calcium (blue) and barium (gray) currents in 10 mM EGTA at V_{max} of tsA201 cells expressing $Ca_V1.2$. The significant difference in I_{res250}/I_{pk} in calcium and barium indicates robust CDI (****$P < 0.0001$, unpaired *t* test).

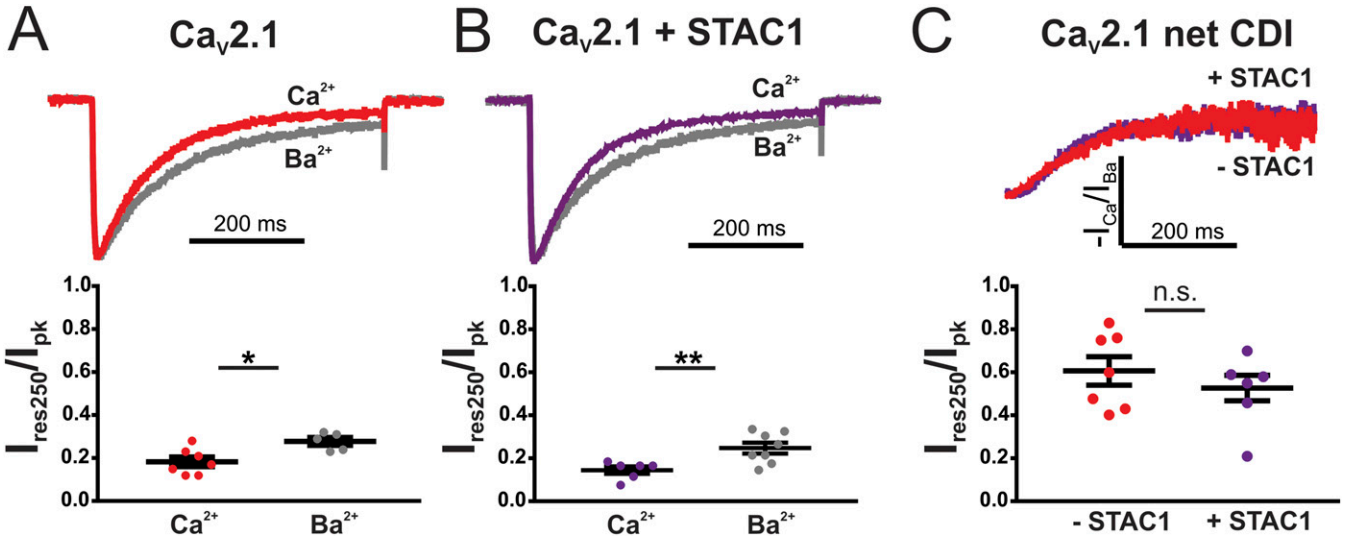

Fig. S5. STAC1 does not affect the CDI of $Ca_V2.1$. Representative normalized calcium (red) and barium (gray) $Ca_V2.1$ currents evoked by a 500-ms depolarization step from a holding potential of −80 mV to V_{max} in the absence (*A*) or presence of STAC1 (*B*) with 0.5 mM EGTA internal calcium buffering. In both conditions $Ca_V2.1$ exhibits CDI (*$P = 0.012$ in *A*, and **$P = 0.009$ in *B*). (*C*) Analysis of the net CDI of $Ca_V2.1$ indicated that coexpression of STAC1 does not alter the CDI of $Ca_V2.1$ (n.s., $P = 0.40$, unpaired *t* test).

Table S1. Biophysical properties of $Ca_V1.2$, $Ca_V1.2$-III-IV_A, and II-III_M in dysgenic myotubes

Parameter	$Ca_V1.2$	$Ca_V1.2$-III-IV_A	$Ca_V1.2$-II-III_M
$V_{0.5}$, mV	10.82 ± 2.49	15.75 ± 3.33	ND
V_{rev}, mV	79.83 ± 1.15	69.87 ± 3.33	ND
I_{max}, pA/pF	−11.34 ± 1.54	−2.46 ± 1.54	−0.07 ± 0.03
G_{max}, nS/pF	0.24 ± 0.03	0.07 ± 0.03	ND
K_a, mV	7.55 ± 0.51	21.93 ± 14.30	ND
n	5	5	5

Half-maximal activation ($V_{0.5}$), reversal potential (V_{rev}), maximal current (I_{max}) and maximal conductance (G_{max}) and slope factor values (k_a) for the measured $Ca_V1.2$ chimeras. Mean values ± SEM. ND, not determined.

Table S2. STAC3-GFP association to $Ca_V1.2$ IQ mutants

IQ mutation	STAC3-GFP coclustering (%)
$Ca_V1.2$-Δ1800	95.8 ± 1.3
$Ca_V1.2$-T1644A-Δ1800	97.8 ± 2.2
$Ca_V1.2$-V1645A-Δ1800	91.1 ± 1.1
$Ca_V1.2$-G1646A-Δ1800	92.2 ± 1.1
$Ca_V1.2$-K1647A-Δ1800	83.3 ± 5.8
$Ca_V1.2$-F1648A-Δ1800	**64.4 ± 5.6**
$Ca_V1.2$-Y1649A-Δ1800	91.1 ± 4.4
$Ca_V1.2$-T1651A-Δ1800	98.9 ± 1.1
$Ca_V1.2$-F1652A-Δ1800	85.6 ± 1.1
$Ca_V1.2$-L1653A-Δ1800	90.0 ± 1.9
$Ca_V1.2$-I1654A-Δ1800	**12.2 ± 5.9**
$Ca_V1.2$-Q1655A-Δ1800	97.8 ± 2.2
$Ca_V1.2$-E1656A-Δ1800	85.6 ± 1.1
$Ca_V1.2$-Y1657A-Δ1800	100.0 ± 0.0
$Ca_V1.2$-F1658A-Δ1800	**38.9 ± 8.7**
$Ca_V1.2$-R1659A-Δ1800	**65.6 ± 6.8**
$Ca_V1.2$-K1660A-Δ1800	98.9 ± 1.1
$Ca_V1.2$-F1661A-Δ1800	91.1 ± 4.4
$Ca_V1.2$-K1662A-Δ1800	83.3 ± 5.1
$Ca_V1.2$-K1663A-Δ1800	92.2 ± 4.4
$Ca_V1.2$-R1664A-Δ1800	93.3 ± 3.3
$Ca_V1.2$-K1665A-Δ1800	94.4 ± 2.9

Fraction of myotubes showing STAC3-GFP coclustering for each point mutant. $n = 3$, $n = 90$. ANOVA $F_{(21, 49)} = 32.41$, $P < 0.0001$. In bold are the four mutations that are significantly different from the control (Tukey post hoc analysis, $P < 0.0001$).

Table S3. Inactivation properties

		Calcium		Barium		Net CDI
Calcium buffering	Constructs	I_{res250}/I_{pk}	*n*	I_{res250}/I_{pk}	*n*	I_{res250}/I_{pk}
0.5 mM EGTA	$Ca_V1.2$	0.08 ± 0.02	11	0.42 ± 0.05	15	0.17 ± 0.04
	$Ca_V1.2$ + STAC1	0.23 ± 0.03	8	0.60 ± 0.04	8	0.39 ± 0.05
	$Ca_V1.2$ + STAC2	0.18 ± 0.03	9	0.67 ± 0.07	7	0.28 ± 0.03
	$Ca_V1.2$ + STAC3	0.55 ± 0.04	9	0.54 ± 0.05	7	1.03 ± 0.07
	$Ca_V2.1$	0.05 ± 0.01	5	0.30 ± 0.05	7	0.13 ± 0.02
	$Ca_V2.1$ + STAC3	0.06 ± 0.01	6	0.26 ± 0.07	6	0.19 ± 0.05
	$Ca_V1.2$-IQ_A	0.11 ± 0.02	11	0.49 ± 0.07	10	0.20 ± 0.04
	$Ca_V1.2$-IQ_A + STAC3	0.21 ± 0.03	13	0.64 ± 0.07	7	0.26 ± 0.04
	$Ca_V2.1$	0.18 ± 0.02	7	0.28 ± 0.02	5	0.61 ± 0.07
	$Ca_V2.1$ + STAC1	0.14 ± 0.02	6	0.24 ± 0.03	8	0.52 ± 0.07
10 mM EGTA	$Ca_V1.2$	0.14 ± 0.03	7	0.59 ± 0.06	6	0.22 ± 0.04
	$Ca_V1.2$ + STAC1	0.65 ± 0.06	8	0.70 ± 0.05	7	1.10 ± 0.07
	$Ca_V1.2$ + STAC2	0.57 ± 0.03	7	0.64 ± 0.09	7	0.88 ± 0.05

Data are expressed as mean values ± SEM. I_{res250}/I_{pk} denotes fractional inactivation at 250 ms from a holding potential of −80 mV to V_{max}.

Table S4. GV relationships

		Calcium			Barium		
Calcium buffering	Constructs	$V_{0.5}$ (mV)	K_a (mV)	*n*	$V_{0.5}$ (mV)	K_a (mV)	*n*
0.5 mM EGTA	$Ca_V1.2$	16.7 ± 3.1	10.0 ± 0.6	11	4.9 ± 1.8	7.5 ± 0.4	15
	$Ca_V1.2$ + STAC1	10.2 ± 2.0	8.7 ± 0.7	8	0.4 ± 1.8	5.5 ± 0.7	8
	$Ca_V1.2$ + STAC2	14.3 ± 3.2	9.7 ± 0.9	9	5.9 ± 3.2	7.8 ± 0.5	7
	$Ca_V1.2$ + STAC3	7.8 ± 3.3	8.1 ± 0.7	10	4.0 ± 1.6	7.5 ± 0.5	7
	$Ca_V2.1$	11.4 ± 0.5	4.8 ± 0.2	6	−1.3 ± 1.5	2.9 ± 0.4	7
	$Ca_V2.1$ + STAC3	9.2 ± 2.5	2.8 ± 0.5	6	0.3 ± 1.7	3.8 ± 0.7	6
	$Ca_V1.2$-IQ_A	12.3 ± 1.9	9.8 ± 0.7	11	1.8 ± 2.5	6.9 ± 0.6	10
	$Ca_V1.2$-IQ_A + STAC3	13.5 ± 1.5	8.7 ± 0.6	13	6.2 ± 3.2	6.9 ± 0.6	7
	$Ca_V2.1$	9.6 ± 0.4	3.3 ± 0.3	7	0.4 ± 0.5	3.1 ± 0.3	5
	$Ca_V2.1$ + STAC1	10.5 ± 1.4	3.7 ± 0.2	6	−0.6 ± 1.4	3.7 ± 0.2	8
10 mM EGTA	$Ca_V1.2$	8.7 ± 2.2	8.3 ± 0.5	7	1.0 ± 2.9	6.6 ± 0.7	6
	$Ca_V1.2$ + STAC1	6.8 ± 2.8	6.0 ± 0.6	7	1.0 ± 1.8	5.6 ± 0.5	7
	$Ca_V1.2$ + STAC2	3.0 ± 2.6	6.3 ± 0.8	7	−2.2 ± 1.9	6.1 ± 0.5	7

Half-maximal activation ($V_{0.5}$) and slope factor values (k_a) for the measured channels in the presence or the absence of STAC proteins in barium and calcium. No significant difference was detected for any channel in $V_{0.5}$ or k_a in the absence or the presence of STAC. Data are expressed as mean values ± SEM.